Contents

Chapter 1

Introduction (draft)

Subsurface scattering (SS) is a physical phenomenon that naturally occurs in a wide range of natural materials. Some of the materials that exhibit a strong SS effect in everyday life are milk, human skin and marble. Subsurface scattering is that phenomenon that occurs when light is partially absorbed by an object, bounces inside ("scatters") and finally exits the surface on another point of the material (see Figure 1.1). The phenomenon that results is generally known as *translucency*. We can see some examples of translucency in Figure 1.2

Since the beginning of computer graphics, various attempts have been performed in order to physically model subsurface scattering. Some of these models involve Monte Carlo simulations of the light entering the medium [Pharr and Hanrahan, 2000], other focus on approximating the diffusion of light within the material using an analytical approach [Jensen et al., 2001].

The first model that proposed and analytical approach was the one by Jensen et al. [2001], as an approximation of the radiative transfer equation. This approximation has then been exploited by different authors, in order to account for multi-layered materials [Donner and Jensen, 2005], heterogeneous materials [Wang et al., 2010] and thin surfaces[Wang et al., 2010]. A recent analytical approximation, proposed by Frisvad et al. [2013], extends the approximation in order to account for the directionality of the incoming light.

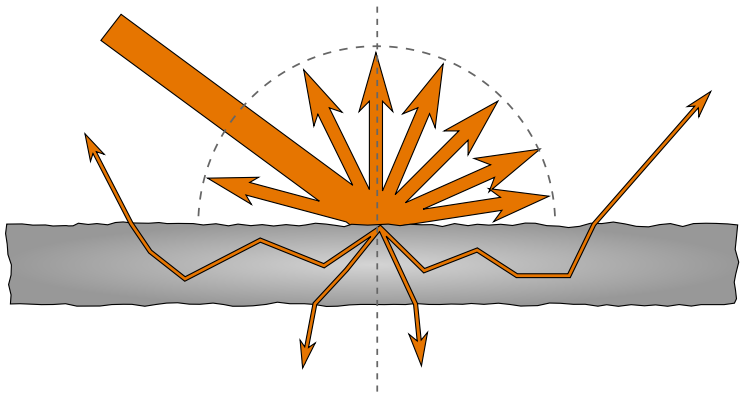

Figure 1.1: Diagram of subsurface scattering. Most of the incoming light gets reflected, but some of it enters the material and leaves it at a different point.

In recent years, with the advent of programmable graphics cards (GPU), it has become possible to exploit these algorithms and bring them to interactive frame rates, and in some cases even to real time rendering. Jensen and Buhler [2002] were the first to propose an efficient implementation (though not real time and on CPU) for rendering subsurface scattering using an octree. More recently, several methods have been proposed, including image-based splats, sum-of-Gaussians filtering, and grid-propagation based methods.

In this thesis we want to employ some cutting edge GPU techniques, with the aid of the programmable pipeline, to implement Frisvad et al. directional model in a real-time fashion. This method should achieve real time results (i.e. in the range of 30 to 60 frames per second) for a wide range of natural materials.

Figure 1.2: Some examples of translucent materials: milk, leaves and a candle. Images courtesy of Wikimedia Commons.

Chapter 2

Related Work

In rendering of subsurface scattering, all approaches rely on approximating correctly the *Radiative Transport Equation* (RTE). We identified two main approaches to the problem in literature:

Analytical One class of solutions consists of approximating the RTE or one of its approximations via an analytical model. These model can have different level of complexity and computation times, and are often adaptable to a wide range of materials. However, often they rely on assumptions on the scattering parameters that limit their applicability.

Numerical In this other class of solutions, a numerical solution for the RTE is actually computed. While providing an exact solution, the computation times are longer. When interactivity is needed, generally some heavy pre computation must be used.

2.1 Analytical techniques

In the analytical techniques, two different areas of research must be distinguished. The first area is the research on the actual models, while the second is

research on how the actual models can be implemented efficiently. Each model is usually represented by a specific function called BSSRDF (*Bidirectional Subsurface Scattering Reflectance Distribution Function*), that describes how light propagates between two points on the surface. This function in the general case must be calculated between all the couple of points on the surface and then integrated over each point. Implementation techniques focus on efficiently implementing this integration step, often making assumptions for which points the computation can be avoided.

2.1.1 Models

Regarding the models, the first and most important is the dipole developed by Jensen et al. [2001]. The models relies on an approximation of the RTE called the *diffusion approximation*, that relies on the assumption on highly scattering materials. In this case, a BSSRDF for a planar surface in a semi-infinite medium can be obtained. The BSSRDF needs only the distance between two points to be calculated, and with some precautions can be also extended to arbitrary geometry. This model does not include any single scattering term, that needs to be evaluated separately. The model was then further extended in order to account for multi-layered materials[Donner and Jensen, 2005].

A significant improvement on the model was later given by D'Eon [2012], that improved the model to better fit path traced simulations without any extra computation cost. A more advanced model based on quantization was proposed by D'Eon and Irving [2011], that introduced a new physical foundation in order to improve the accuracy of the original diffusion approximation. Finally, some higher order approximation exist [Frisvad et al., 2013], in order to account for the directionality of the incoming light and single scattering. This allows a more faithful representation of the model at the price of extended computation times.

Finally, for real-time critical applications (such as games), translucency is often estimated as a function of the thickness of the material, that is used to modify a lambertian term [Tomaszewska and Stefanowski, 2012]. While not physically accurate, this technique allows to have a fast translucency effect that can be easily added to existing deferred pipelines.

2.1.2 Implementations

Most research on efficient implementations of a subsurface scattering analytical model has been made on the original model by Jensen et al. [2001]. The first

efficient implementation was proposed by Jensen and Buhler [2002], based on a two-pass hierarchical integration approach. Samples on the model are organized in an octree data structure, that then is used to render the object. In the first step, the radiance from the light is stored in the points. In the second pass, using the octree, the contribution from neighboring points is computed, clustering far points in order to speed up calculations. In the original paper, the single scattering term is approximated with as a simple BRDF approximation.

Lensch et al. [2002] approached the problem by subdividing the subsurface scattering contribution into two: a direct illumination part and a global illumination part (i.e. the light shining through the object). The global illumination part is pre-computed as vertex-to-vertex throughput and then summed to the direct illumination term in real-time. Translucent shadow maps [Dachsbacher and Stamminger, 2003] use an approach similar to standard shadow maps: they render the scene from the light point of view, and then calculate the dipole contribution in one point only from a selected set of points, according to a specified sampling pattern. As in Lensch et al. [2002], the contribution is split into global and local to permit faster computations. Mertens et al. [2003b] propose a fast technique based on radiosity hierarchical integration techniques, that unlike the previous implementation can handle deformable geometry.

Another important category of methods is screen space methods. Mertens et al. [2003a] propose an image space GPU technique that pre-computes a set of sample points for the area integration and then performs the integral over multiple GPU passes. d'Eon et al. [2007] proposes a method in image-space, interpreting subsurface scattering as a sum of images to which a gaussian filter has been applied. The gaussians are then summed with weights that make them fit the diffusion approximation. Jimenez et al. [2009] improves further the technique, giving more precise results in case of skin. Shah et al. [2009] present a fast technique that render the object as a series of splats, using GPU blending to sum over the various contributions.

Regarding more advanced models, the better and the quantized dipole can be applied to any of the previous implementations, since they do not require additional information that the standard dipole. On the other hand, the directional dipole requires the direction of the incoming light as part of its calculations, so it is generally not applicable to the mentioned implementations.

2.2 Numerical techniques

Numerical techniques for subsurface scattering are often not specific, but come for free or as an extension of a global illumination numerical approximation, since the governing equations are essentially the same. Given their generality, they are usually slower that their analytical counterpart, and often rely on heavy pre-computation steps in order to achieve interactive framerates. Jensen's Photon Mapping[Jensen and Christensen, 1998] was originally developed to render anisotropic subsurface scattering. Classical approaches as a full Monte-Carlo simulation implementation of the light-material interaction[Dorsey et al., 1999], and finite-difference methods exist in literature[Stam, 1995].

Some less general methods have been introduced in order to devise more efficient approximations when it comes to the specific problem of subsurface scattering. Stam [1995] uses the diffusion approximation with the finite difference method on the object discretized on a 3D grid. Fattal [2009] uses as well a 3D grid, that is swept with a structure called light propagation map, that stores the intermediate results until the simulation is complete.

Wang et al. [2010], instead of performing the simulation on a discretized 3D grid, makes the propagation directly in the mesh, converting it into a connected grid of tetrahedrons called *QuadGraph*. This grid can be optimized to be GPU cache friendly, and provide a real-time rendering of deformable heterogeneous objects. The problem in this method is that the QuadGraph is slow to compute (20 minutes for very complex meshes) and has heavy memory requirements for the GPU.

Precomputed radiance transfer methods is another class of general global illumination methods, that generally pre-compute part of the lighting and store it in tables[Donner et al., 2009], allowing to retrieve it efficiently with an additional memory cost.

A recent method called SSLPV - Subsurface Scattering Light Propagation Volumes [Børlum et al., 2011] extends a technique originally developed by Kaplanyan and Dachsbacher [2010] to propagate light efficiently in a scene using a set of discretized directions on a 3D grid. The method allows real-time execution times and deformable meshes with no added pre-computation step, with the drawback of not being physically accurate.

Chapter 3

Theory

In this chapter, we give a theoretical introduction to the topic dealt with in this thesis. The ultimate goal of this chapter is to introduce and describe what a analytical model for subsurface scattering is. First, we will give a brief introduction to what light is, and how we physically describe it. Secondly, we will introduce the basic radiometric quantities that will be used throughout the chapter. Then, we will describe how this quantities are related and can be used to describe light-material interaction, using reflectance functions, of which BSSRDF functions are a special case. Finally, we will introduce subsurface scattering and the diffusion approximation, concluding with a description of two BSSRDF functions actually used to describe it, by Jensen et al. [2001] and Frisvad et al. [2013].

3.1 Light and Radiometry

Light is a form of electromagnetic radiation, that propagates through space as a sinusoidal wave. Usually by *light* we usually refer to *visible light*, the small part of the electromagnetic spectrum the human eye is sensible to (see Figure 3.1). This small window is between the 380 nm of infrared and 750 nm of ultraviolet light, but the precise boundaries vary according to the environment and the

observer. Instead explicitly noted, we will use the terms light and visible light interchangeably in this report.

The study of light is usually referred as *optics*. In computer aided image synthesis, we are interested in representing faithfully how visible light propagates through a scene and how interacts with the objects and the materials in it. In addition, we are interested in lighting effects that are noticeable at human scales (1 mm - 1 km). For example, we are interested in subsurface scattering, absorption and emission phenomena but not in diffraction, interference and quantum effects, that for visible light happen on a microscopic scale (1 nm - 1 µm).

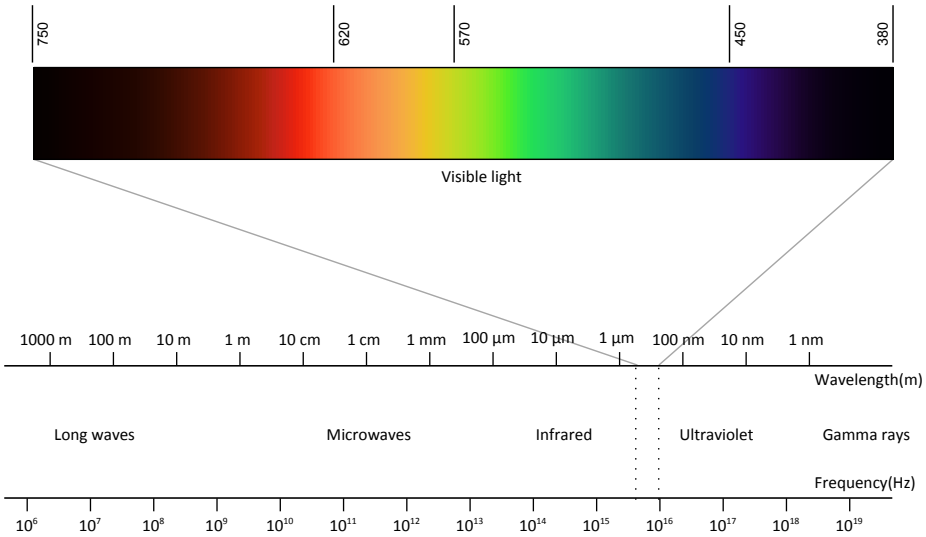

Figure 3.1: The electromagnetic spectrum.

The branch of physics that studies how to measure electromagnetic radiation is called *radiometry*. The energy of light, like all the others forms of energy, is measured in *Joules* [J = $\mathrm{kg\,m\,s^{-2}}$], and its power in *Watts* [W = $\mathrm{kg\,m\,s^{-3}}$]. *Photometry*, on the other hand, measures electromagnetic radiation as it is perceived from the human eye, and limits itself only to the visible spectrum, while radiometry spans all of it. The corresponding names for energy and power in photometry are *radiant energy*, measured in *talbots* [cd s], and *radiant flux*, measured in *candelas* [cd].

In image synthesis radiometry is usually employed, as its quantities directly derive from the electromagnetic theories, are universal, and can be easily converted to the photometric ones when necessary. The most important radiometric quantities used in computer graphics are *radiant flux*, *radiant energy*, *radiance*, *irradiance* and *intensity*.

3.2 Radiometric quantities

3.2.1 Radiant flux

The radiant flux, also known as radiant power, is the most basic quantity in radiometry. It is usually indicated with the letter Φ and it is measured in joules per seconds [$\mathrm{J\,s^{-1}}$] or Watts [W]. The quantity indicates how much power the light irradiates per unit time.

3.2.2 Radiant energy

Radiant energy, usually indicated as Q, is the energy that the light carries in a certain amount of time. Like all the other SI units for energy, it is measured in joules [J]. Radiant energy is obtained integrating the radiant flux along time for an interval ΔT:

$$Q = \int_{\Delta T} \Phi \, dt$$

Due to the dual nature of the light, the energy carried by the light can be derived both considering the flux of photons as particles, or considering light as a wave. We will not dig further into the topic, because for rendering purposes is not important if we characterize light as a flux of particles or as a sinusoidal wave.

3.2.3 Irradiance

Irradiance, usually defined as E, is the radiometric unit that measures the radiant flux per unit area *falling* on a surface. It is measured in Watts per square meter [$\mathrm{W\,m^{-2}}$]. It is obtained by further deriving the radiant flux by the area:

$$E = \frac{d\Phi}{dA}$$

Irradiance is usually the term in literature used for the *incoming* power per unit area. The converse, i.e. the irradiance leaving a surface, it is usually referred as *radiant exitance* or *radiosity*, and indicated with the letter B.

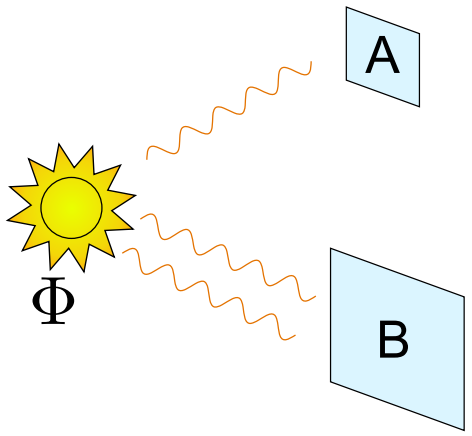

Figure 3.2: Irradiance versus power. For the two surfaces A and B, the received power Φ is the same, while the two irradiances E_A and E_B are different, as the area of B is twice as the one of A.

3.2.4 Intensity

Intensity is defined as the differential radiant flux per differential solid angle:

$$I(\vec{\omega}) = \frac{d\Phi}{d\omega}$$

It is measured in Watts per steradian [$\mathrm{W\,sr^{-1}}$] and it is indicated with the letter I. Intensity is often a misused term in the physics community, as it is used for many different measures. Depending on the community, intensity may refer to irradiance or even to radiance (see the following section). We will refer to intensity as it is generally interpreted by the optics community, i.e. radiant intensity.

3.2.5 Radiance

Radiance is the most important quantity in image synthesis. It is defined precisely as the differential of the flux per solid angle per projected surface area, and it is measured in Watt per steradian per square meter [$\mathrm{W\,sr^{-1}\,m}$].

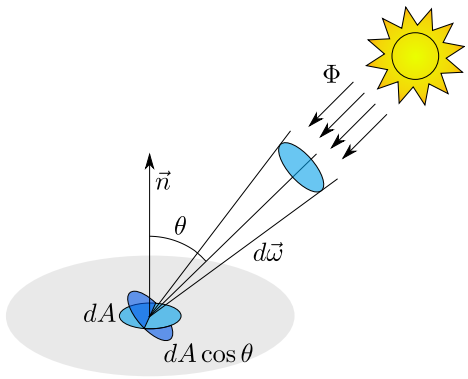

Figure 3.3: Radiance. The element of area dA gets projected according to the angle $\theta = \cos^{-1}\vec{n}\cdot\vec{\omega}$. Then the incoming flux Φ gets divided by the projected area and by the solid angle subtended by it.

$$L(\vec{\omega}) = \frac{d^2\Phi}{d\omega dA\cos\theta}$$

Where θ is the angle between the surface normal and the incoming ray of light (so that $\cos\theta = \vec{n}\cdot\vec{\omega}_i$). Radiance is important in image synthesis because it is the natural quantity to associate with a ray of light, as it remains constant along it. In addition, the sensibility of the human eye to light is directly proportional to the radiance. For a discussion on why radiance is related to the sensitivity of sensors and the human eye, see Cohen et al. [1993].

All the other radiometric quantities can be derived from radiance:

$$\begin{aligned} E &= \int_{2\pi} L_i(\vec{\omega})\cos\theta\ d\omega \\ B &= \int_{2\pi} L_o(\vec{\omega})\cos\theta\ d\omega \\ I(\vec{\omega}) &= \int_{A} L(\vec{\omega})\cos\theta\ dA \\ \Phi &= \int_{A}\int_{2\pi} L(\vec{\omega})\cos\theta\ d\omega dA \end{aligned} \tag{3.1}$$

For simplicity of notation, in the previous formulas the dependence from the point of incidence $\mathbf{x}$ has been dropped. In principle, all the quantities listed in equation 3.1 are dependent on $\mathbf{x}$.

3.2.6 Radiometric quantities for simple lights

To help with the formulas used later in the report, we derive the standard radiometric quantities for the two simplest types of light, i.e. directional and point lights.

- *Directional lights* simulate very distant light sources, in which all the rays of light are parallel (e.g. the sun). They are represented by a direction $\vec{\omega}_l$ and a constant radiance value, L.
- *Point lights* simulate lights closer to the observer. Isotropic point lights are represented by a position of the light $\mathbf{x}_l$ and a constant intensity I. Point lights have a falloff that depends on the inverse square law, i.e. the radiance diminishes with the square of the distance.

Table 3.1 shows different radiometric quantities evaluated for point and directional lights, for a surface point $\mathbf{x}$ with surface normal $\vec{n}$.

Quantity	Directional light	Point light
Cosine term	$\cos\theta = \vec{n} \cdot \vec{\omega}_l$	$\cos\theta = \frac{(\mathbf{x}-\mathbf{x}_l)\cdot\vec{n}}{\lvert\mathbf{x}-\mathbf{x}_l\rvert}$
$\Phi(\mathbf{x})$ Flux	$L\ \delta(\vec{\omega})$	$4\pi I$
$E(\mathbf{x})$ Irradiance	$L\cos\theta$	$I\frac{\cos\theta}{\lvert\mathbf{x}_l-\mathbf{x}\rvert^2}$
$I(\mathbf{x},\vec{\omega})$ Intensity	$L\ \delta(\vec{\omega})$	I
$L(\mathbf{x},\vec{\omega})$ Radiance	L	$\frac{I}{\lvert\mathbf{x}_l-\mathbf{x}\rvert^2}$

Table 3.1: Different radiometric values for simple light sources.

3.3 Reflectance Functions

After introducing the basic radiometric quantities, we still lack a rigorous way to describe light material interaction. More precisely, we need a way to relate the incoming and the outgoing radiance on a point of a chosen surface. As we have already discussed before, we use radiance since is the radiometric quantity that is directly proportional to what the human eye perceives.

3.3.1 BRDF functions

One of the possible way to describe light-material interaction is by using a BDRF function, acronym for *Bidirectional Reflectance Distribution Function*. The BRDF function $f(\mathbf{x}, \vec{\omega}_i, \vec{\omega}_o)$ is defined on one point $\mathbf{x}$ of the surface as the differential ratio between the exiting radiance and the incoming irradiance:

$$f(\mathbf{x}, \vec{\omega}_i, \vec{\omega}_o) = \frac{dL_o(\mathbf{x}, \vec{\omega}_o)}{dE_i(\mathbf{x}, \vec{\omega}_i)} = \frac{dL_o(\mathbf{x}, \vec{\omega}_o)}{L_i(\mathbf{x}, \vec{\omega}_i) \cos\theta_i d\vec{\omega}_i} \tag{3.2}$$

The BRDF states that the incoming and the outgoing radiance are proportional, so that the energy hitting the material at the point $\mathbf{x}$ is proportional to the energy coming out from the point. The BRDF function has the following properties:

- *reciprocal* for the Hemholtz reciprocity principle, a physics result that is also the basis of reverse path ray tracingDesolneux et al. [2007]:

$$f(\mathbf{x}, \vec{\omega}_i, \vec{\omega}_o) = f(\mathbf{x}, \vec{\omega}_o, \vec{\omega}_i)$$

- *anisotropic*, as if the surface changes orientation and $\vec{\omega}_i$ and $\vec{\omega}_o$ stays the same, the resulting BRDFs are different. So generally

$$f(\mathbf{x}, \vec{\omega}_i, \vec{\omega}_o) \neq f(\mathbf{x}, \vec{\omega}_o + \vec{\omega}, \vec{\omega}_i + \vec{\omega})$$

- *positive*, as otherwise it would mean that either the power or the irradiance are negative.

$$f(\mathbf{x}, \vec{\omega}_o, \vec{\omega}_i) \geq 0$$

- *energy conserving*, so that the energy of the outgoing ray is no grater that the one of the incoming one

$$\int_{2\pi} f(\mathbf{x}, \vec{\omega}_o, \vec{\omega}_i) \cos\theta_o d\vec{\omega}_o \leq 1$$

By inverting equation 3.2, we obtain the so-called *reflectance equation*:

$$L_o(\mathbf{x}, \vec{\omega}_o) = \int_{2\pi} f(\mathbf{x}, \vec{\omega}_i, \vec{\omega}_o) L_i(\mathbf{x}, \vec{\omega}_i) \cos\theta_i d\vec{\omega}_i$$

Later we will use this equation as a starting point to obtain the full rendering equation. The BRDF function has some limitations, being not able to account for all phenomena. For example, with a BRDF it is not possible to account for subsurface scattering phenomena, because it assumes the light enters and leaves the material at the same point. To model these phenomena, more complicated functions are needed, like the BSSRDF function described later in this chapter.

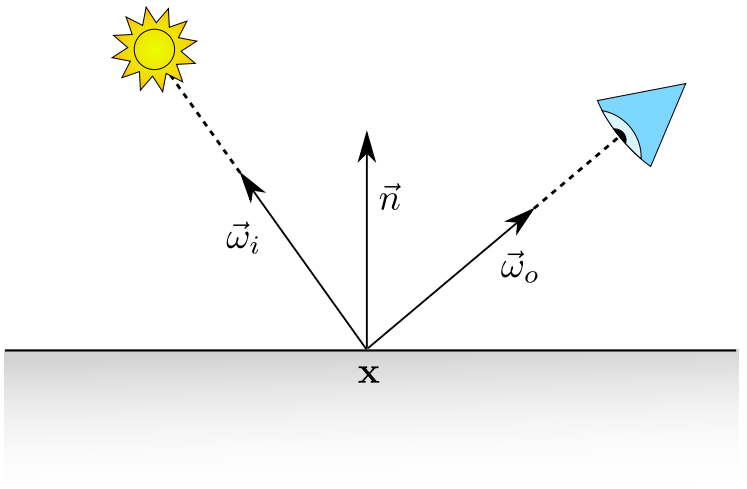

Figure 3.4: Setup for a BRDF. Note that the light enters and leaves the surface at the same point.

3.3.2 Examples of BRDF functions

3.4 Light transport and subsurface scattering

There are many examples of BRDF functions in literatureMontes Soldado and Ureña Almagro [2012]. In this section, we will introduce three of the simplest ones: for a more exhaustive description of BRDF functions, refer to TODO. The three BRDFs are the lambertian or diffuse BRDF, the specular or mirror BRDF and the family of glossy BRDFs.

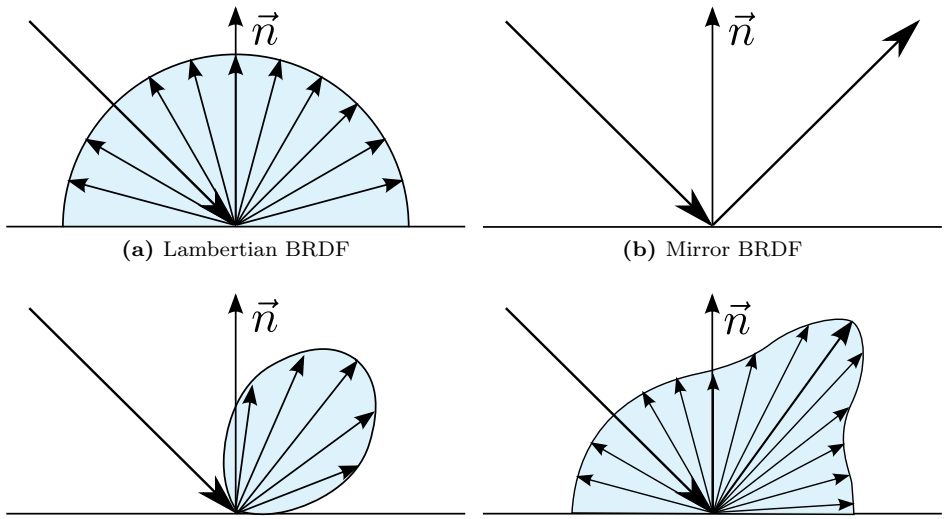

(a) Lambertian BRDF **(b)** Mirror BRDF

(c) Glossy BRDF **(d)** Combined BRDF

Figure 3.5: Examples of BRDF functions. In this particular example, the three simple BRDFs can be combined in the more complex BRDF of figure **??** in order to combine multiple effects.

3.4.0.1 Lambertian BRDF

In the lambertian BRDF, the incoming radiance is distributed equally in all directions, regardless of the incoming direction. To do this, the BRDF must be constant:

$$f(\mathbf{x}, \vec{\omega}_i, \vec{\omega}_o) = k_d$$

We can check that then the radiance is scattered equally in all directions by simple integration:

$$\begin{aligned} L_o(\mathbf{x}, \vec{\omega}_o) &= \int_{2\pi} f_d L_i(\mathbf{x}, \vec{\omega}_i) \cos\theta_i d\vec{\omega}_i \\ L_o(\mathbf{x}, \vec{\omega}_o) &= k_d \int_{2\pi} L_i(\mathbf{x}, \vec{\omega}_i) \cos\theta_i d\vec{\omega}_i \\ L_o(\mathbf{x}, \vec{\omega}_o) &= k_d \; E(\mathbf{x}) \end{aligned}$$

The lambertian model is an ideal model, so very few material exhibit a lambertian diffusion, like unfinished wood or spectralon, a synthetic material created in order to have a lambertian diffusion.

3.4.0.2 Mirror BRDF

Another simple kind of BRDF is the perfectly specular BRDF, or mirror BRDF. In this function, all the incoming radiance from one direction $\vec{\omega}_i$ is completely diffused into the reflected direction $\vec{\omega}_r$, defined as $\vec{\omega}_r = \vec{\omega}_i - 2(\vec{\omega}_i \cdot \vec{n})\vec{n}$. The resulting BRDF is defined as follows:

$$f(\mathbf{x}, \vec{\omega}_i, \vec{\omega}_o) = \frac{\delta(\vec{\omega}_o - \vec{\omega}_r)}{\cos\theta_i}$$

The function $\delta(\vec{\omega})$ is a hemispheric delta function. Once integrated over a hemisphere, the function evaluates to one only for the vector $\vec{\omega} = \mathbf{0}$. Putting the BRDF into the reflectance equation gives the following outgoing radiance:

$$L_o(\mathbf{x}, \vec{\omega}_o) = \begin{cases} L_i(\mathbf{x}, \vec{\omega}_i) & \text{if } \vec{\omega}_o = \vec{\omega}_r \\ 0 & \text{otherwise} \end{cases}$$

that is the expected result, as all the radiance is reflected into the direction $\vec{\omega}_r$.

3.4.0.3 Glossy BRDFs

As we can see from real life experience, rarely objects are completely diffuse or completely specular. These two models are idealized models, that represent an ideal case. So, to create a realistic BRDF model, we often need to combine the two terms and add an additional one, called glossy reflection. This term is often needed to model the behavior of the surface more realistically, especially at grazing angles.

The most used BRDF model used to model glossy reflections is based on microfacet theory Ashikmin et al. [2000]. In this theory, the surface of an object is modeled as composed of small mirrors. In one of its classical formulation, the BRDF is represented as:

$$f(\mathbf{x}, \vec{\omega}_i, \vec{\omega}_o) = \frac{DGR}{4\cos\theta_r \cos\theta_i} = \frac{GR}{4}\frac{(\vec{n}\cdot\vec{h})^s}{(\vec{n}\cdot\vec{r})(\vec{n}\cdot\vec{\omega}_i)}$$

D regulates how microfacets are distributed, and it is often modeled as $(\vec{n}\cdot\vec{h})^s$, where $\vec{h}$ is the half vector between the eye and the light, and s is an attenuation parameter. $\vec{h}$ is defined as:

$$\vec{h} = \frac{\vec{\omega}_o + \vec{\omega}_i}{\|\vec{\omega}_o + \vec{\omega}_i\|}$$

G accounts for the object self shadowing, while R is the Fresnel reflection term (more details in section 3.4.2). $\vec{r}$ is the reflection vector as defined in the previous section. See figure Z on how the vectors for the glossy reflection - $\vec{n}$, $\vec{h}$ and $\vec{r}$ - are defined.

Various alternative definitions exist for the D and G function, varying among the literature. Other glossy models not based on microfacet theory do exist as well Montes Soldado and Ureña Almagro [2012].

3.4.1 The rendering equation

Given the reflectance equation, it is possible to generalize it in order to model all the lighting in an environment. In fact, the described reflectance equation is a suitable candidate to represent a full global illumination model, but it does not account for two important factors.

The first factor are emissive surfaces. We need to add an emissive radiance term $L_e(\mathbf{x}, \vec{\omega})$ that models how much radiance is a point on a surface emitting in a certain directions. This is useful to model lights as any other surface in the scene. Note that point lights have a singularity: they emit infinite radiance on the point they are placed.

The second factor is that the reflectance equation accounts only for direct illumination. In general, we want to model global illumination, i.e. to include also light that bounced onto another surface before reaching the current surface. To model this, we can replace the L_i term in the reflectance equation with another term L_r that accounts for light coming from another surface. This term can be usually modeled as the product of the radiance of the light plus a visibility function $V(\mathbf{x})$.

Accounting for all the described factors, we reach one formulation of the rendering equation:

$$L_o(\mathbf{x}, \vec{\omega}_o) = L_e(\mathbf{x}, \vec{\omega}) + \int_{2\pi} f(\mathbf{x}, \vec{\omega}_i, \vec{\omega}_o) L_i(\mathbf{x}, \vec{\omega}_i) V(\mathbf{x}) \cos\theta_i d\vec{\omega}_i$$

This form of the rendering equation is still not completely general, since it is based on a BRDF, so it is not possible to model subsurface scattering effects or wavelength-changing effects (like iridescence). We will extend the rendering equation in order to account for these phenomena later on in this chapter.

3.4.2 Fresnel equations

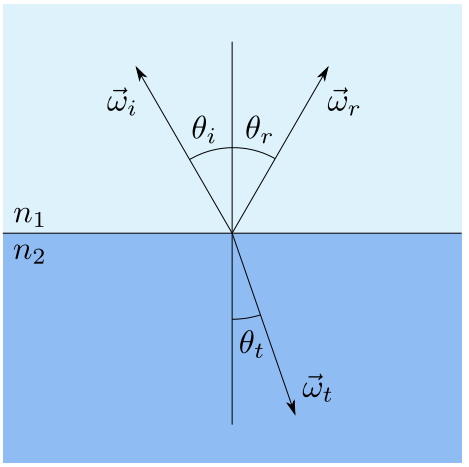

Figure 3.6: Reflected and refracted vector on mismatching indices of reflection.

Until now, on the described BRDF models, we did consider only the reflected part of the radiance. When a beam of light coming from direction $\vec{\omega}_i$ hits a surface, only part of the incoming radiance gets reflected, while another part gets refracted into the material. As we can see from the setup from figure Z, we obtain the two vectors $\vec{\omega}_r$ and $\vec{\omega}_t$, the reflected and refracted vector, defined as follows:

$$\vec{\omega}_r = \vec{\omega}_i - 2(\vec{\omega}_i \cdot \vec{n})\vec{n}$$
$$\vec{\omega}_t = \eta((\vec{\omega}_i \cdot \vec{n})\vec{n} - \vec{\omega}_i) - \vec{n}\sqrt{1 - \eta^2(1 - (\vec{\omega}_i \cdot \vec{n})^2)}$$

Where $\eta = \frac{n_1}{n_2}$ is the relative index of refraction of the material. With this setup, illustrated in figure 3.6, we can use a solution to Maxwell's equations for wave propagation to describe how light spreads between reflected and refracted directions. What we obtain are called *Fresnel coefficients*. The coefficients are different according to the polarization of the incoming light, so there are two for the reflection (R_s, R_p) and two for transmission (T_s, T_p). The coefficients relate the incoming and outgoing power of the light, and by differentiation, the radiance as well.

$$
\begin{aligned}
R_s(\eta, \vec{\omega}_i) &= \left| \frac{\eta \cos\theta_i - \cos\theta_t}{\eta \cos\theta_i + \cos\theta_t} \right|^2 \\
R_p(\eta, \vec{\omega}_i) &= \left| \frac{\eta \cos\theta_t - \cos\theta_i}{\eta \cos\theta_t + \cos\theta_i} \right|^2 \\
T_s(\eta, \vec{\omega}_i) &= \eta \, \frac{\cos\theta_t}{\cos\theta_i} \left| \frac{2\cos\theta_i}{\eta \cos\theta_i + \cos\theta_t} \right|^2 \\
T_p(\eta, \vec{\omega}_i) &= \eta \, \frac{\cos\theta_t}{\cos\theta_i} \left| \frac{2\cos\theta_i}{\eta \cos\theta_t + \cos\theta_i} \right|^2
\end{aligned}
$$

In most computer graphics applications (and this is reasonable for most of the real-world lights), we assume that the two polarizations are equally mixed. So, we will use the coefficient $R = \frac{R_s + R_p}{2}$ and $T = \frac{T_s + T_p}{2}$ in our calculations. Note that $R + T = 1$, so the overall energy is conserved.

3.4.3 BSSRDF functions and generalized rendering equation

As we anticipated in section 3.3.1, the BRDF theory that was introduced before is not accurate in predicting the behavior in the lighting for all materials. In fact, BRDF models assume that the light enters and leaves the material in the same point. While this assumption holds true for a wide range of material, like metal or plastic, it poorly describes translucent materials, that exhibit a consistent amount of light transport under the surface.

In order to describe light transport in this material, we introduce a function, called BSSRDF, acronym for *Bidirectional Subsurface Scattering Reflectance Distribution Function*. This function extends the concept of BRDF to account for two separate points. The BSSRDF is usually indicated with a capital S. We

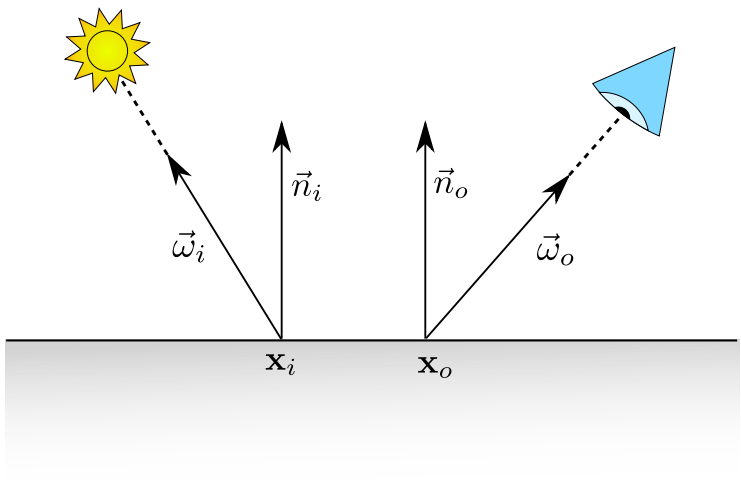

Figure 3.7: BSSRDF setup. As we compare it to the one of figure 3.4, we can see that the light enters and leaves the surface at two different points.

define the BRDF as the ratio between the incoming flux in a point $\mathbf{x}_i$ from the direction $\vec{\omega}_i$ and the outgoing radiance in *another* point $\mathbf{x}_o$ on direction $\vec{\omega}_o$:

$$S(\mathbf{x}_i, \vec{\omega}_i, \mathbf{x}_o, \vec{\omega}_o) = \frac{dL_o(\mathbf{x}_o, \vec{\omega}_o)}{d\Phi_i(\mathbf{x}_i, \vec{\omega}_i)} = \frac{dL_o(\mathbf{x}_o, \vec{\omega}_o)}{dE_i(\mathbf{x}_i, \vec{\omega}_i)dA_i} = \frac{dL_o(\mathbf{x}_o, \vec{\omega}_o)}{L_i(\mathbf{x}_i, \vec{\omega}_i)\cos\theta_i d\vec{\omega}_i dA_i}$$

As we can see, the BSSRDF is similar to the BRDF, apart from a additional derivation in the area domain. Once we rearrange this equation, we can obtain an updated reflectance equation for the BSSRDF:

$$L_o(\mathbf{x}_o, \vec{\omega}_o) = \int_A \int_{2\pi} S(\mathbf{x}_i, \vec{\omega}_i, \mathbf{x}_o, \vec{\omega}_o) L_i(\mathbf{x}_i, \vec{\omega}_i) \cos\theta_i d\vec{\omega}_i dA_i$$

We can immediately see that the new reflectance equation accounts for light scattering between two points, but with a price. In fact, it adds a order of magnitude of complexity, since now the BSSRDF needs to be integrated on the whole surface and on the normal hemisphere, while the BRDF needed only a integration over the hemisphere.

As we did for the BRDF, we can further extend the reflectance equation to further include visibility and emission, giving an extended form of the rendering

equation.

$$L_o(\mathbf{x}_o, \vec{\omega}_o) = L_e(\mathbf{x}_i, \vec{\omega}_i) + \int_A \int_{2\pi} S(\mathbf{x}_i, \vec{\omega}_i, \mathbf{x}_o, \vec{\omega}_o) L_i(\mathbf{x}_i, \vec{\omega}_i) V(\mathbf{x}) (\vec{n} \cdot \vec{\omega}_i) d\vec{\omega}_i dA_i \tag{3.3}$$

From now on, by "rendering equation" in this report we will mean the one in equation 3.3.

3.5 Light transport and subsurface scattering

When we derive our models for lighting, in general we assume that the light is traveling in vacuum. This assumption holds for light that is propagating though the air (which is assimilable to vacuum), but once we relax it, more variables should be taken into consideration. Objects through which light travels are referred as *participating media*. In this chapter, we will derive and consider an alternative formulation of the rendering equation for light traveling into participating media, called *radiative transport equation*.

When a beam of light travels through an object, various phenomena occur. A photon on the beam can be either being absorbed (disappear), scattered (change direction) or emitted (appear). These phenomena can be uniform throughout the material (homogeneous materials), as in solid material like wax or leaves, or be not uniform (heterogeneous materials), like in smoke or clouds.

We will briefly describe all three mentioned effects, then combine them to compose the radiative transport equation. The purpose is to describe how radiance varies along a beam of light with direction $\vec{\omega}$. This directional derivative is indicated as:

$$(\vec{\nabla} \cdot \vec{\omega}) L(\mathbf{x}, \vec{\omega}) = \frac{\partial L_x}{\partial x} \vec{\omega}_x + \frac{\partial L_y}{\partial y} \vec{\omega}_y + \frac{\partial L_z}{\partial z} \vec{\omega}_z$$

3.5.1 Emission

Emission is the natural property of the materials to emit light, i.e. to generate photons that add to the existing ones passing through the material. The effect

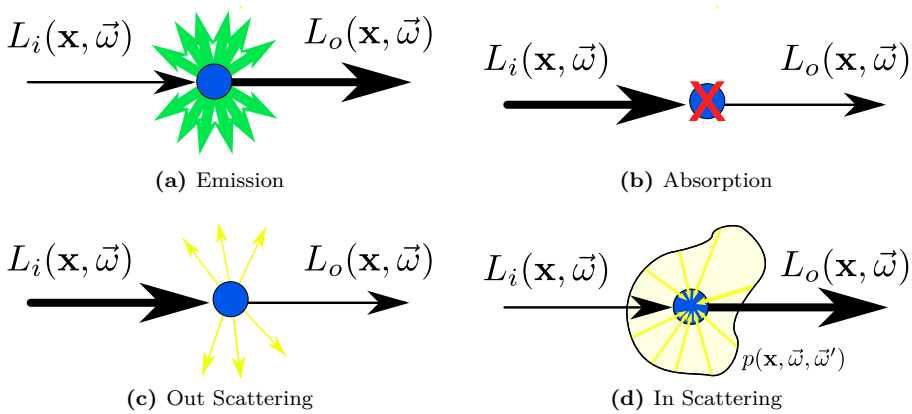

(a) Emission **(b)** Absorption

(c) Out Scattering **(d)** In Scattering

is generally generated by chemical processes emitting photons (as in natural animals like fireflies), by natural black-body radiation emission in the visible spectrum (such as in a star like the sun or in incandescent bulbs), or by other radiation that changed its wavelength into the visible spectrum.

In the directional 3D derivative, the variance in emission is modeled as a constant depending only on the current position and direction:

$$(\vec{\nabla} \cdot \vec{\omega}) L(\mathbf{x}, \vec{\omega}) = \epsilon(\mathbf{x}, \vec{\omega})$$

This means that emission increases linearly along the body: if the beam travels a distance d within the medium, $d \cdot k$ photons are emitted. Emission is generally isotropic, not depending on the direction ($\epsilon(\mathbf{x}, \vec{\omega}) = \epsilon(\mathbf{x})$).

3.5.2 Absorption

Absorption is a property of materials that models a simple physical phenomenon: a photon, traveling though the material, hits one atom of the material. The energy carried by the photon is then absorbed by the atom, augmenting its kinetic energy. This directly translates in an increase of heat in the material. Usually a certain percentage of the photons hits the atoms and gets absorbed. This means, if k is the percentage of the photons absorbed in a unit, after one unit the original radiance will become $k \cdot L_i$, then $k^2 \cdot L_i$, etc.

If we write this phenomena as a differential equation, we get after a distance d a radiance reduction of $k^d = e^{-\sigma_a d}$, that leads to the following 3D directional derivative:

$$(\vec{\nabla} \cdot \vec{\omega})L(\mathbf{x}, \vec{\omega}) = -\sigma_a(\mathbf{x}, \vec{\omega})L(\mathbf{x}, \vec{\omega})$$

σ_a is referred as the *absorption coefficient*. Also this coefficient is generically isotropic, and constant for homogenous materials.

3.5.3 Out-scattering

Out scattering is the radiance lost due to scattering. The scattering phenomenon happens when photons are deflected away from the current direction $\vec{\omega}$. As in the previous case, the phenomena is modeled as a percentage of the radiance lost per unit length. So the loss due to out-scattering is modeled as:

$$(\vec{\nabla} \cdot \vec{\omega})L(\mathbf{x}, \vec{\omega}) = -\sigma_s(\mathbf{x}, \vec{\omega})L(\mathbf{x}, \vec{\omega})$$

σ_s is referred as the *scattering coefficient*. We note that in this case we are not interested in which direction the photons are actually going. That will be accounted in the in-scattering term of another point in the material.

3.5.4 In-scattering

Given some loss due to some of the photons changing direction, there will be some of them that from other scattering events will change to the $\vec{\omega}$ direction. We need then to discover the number of photons that comes from all the other directions. To do this, we integrate the incoming radiance from all directions in the point $\mathbf{x}$. This quantity, similar to irradiance, in an infinite medium is called *fluence*, and indicated as ϕ:

$$\phi(\mathbf{x}) = \int_{4\pi} L(\mathbf{x}, \vec{\omega}')d\omega'$$

This quantity should be then averaged over the entire sphere, yielding $\frac{\phi}{4\pi}$ as a result. This quantity then is then multiplied by the scattering coefficient,

because only some photons on average align to the current direction $\vec{\omega}$. This yields:

$$(\vec{\nabla} \cdot \vec{\omega})L(\mathbf{x}, \vec{\omega}) = \sigma_s(\mathbf{x})\frac{1}{4\pi}\int_{4\pi} L(\mathbf{x}, \vec{\omega}')d\omega' \tag{3.4}$$

However, equation 3.4 assumes that radiance scatters equally in all directions. This is not usually the case, and the $\frac{1}{4\pi}$ term needs to be replaced by a probability distribution function that describes how the photons scatter in the medium. This function is called phase function, and indicated as $p(\mathbf{x}, \vec{\omega}, \vec{\omega}')$. In the actual models its integral on the hemisphere is often used as a parameter, called *mean cosine* (g):

$$g(\mathbf{x}) = \int_{4\pi} p(\mathbf{x}, \vec{\omega}, \vec{\omega}')\vec{\omega} \cdot \vec{\omega}' d\omega'$$

This term indicates the general direction of the scattering in the material. If positive, the scattering is prevalent along the beam (forward scattering), if negative is prevalent in the opposite direction (backward scattering). If zero, the scattering is isotropic, i.e. equal in all directions.

So, the final 3D equation for in-scattering, accounting for the phase function, is as follows:

$$(\vec{\nabla} \cdot \vec{\omega})L(\mathbf{x}, \vec{\omega}) = \sigma_s(\mathbf{x})\int_{4\pi} p(\mathbf{x}, \vec{\omega}, \vec{\omega}')L(\mathbf{x}, \vec{\omega}')d\omega'$$

3.5.5 Final formulation of the radiative transport equation

Combining emission, absorption, scattering described in the previous sections, we reach the final formulation of the radiative transport equation (RTE):

$$(\vec{\nabla} \cdot \vec{\omega})L(\mathbf{x}, \vec{\omega}) = -\sigma_t(\mathbf{x})L(\mathbf{x}, \vec{\omega}) + \epsilon(\mathbf{x}) + \sigma_s(\mathbf{x})\int_{4\pi} p(\mathbf{x}, \vec{\omega}, \vec{\omega}')L(\mathbf{x}, \vec{\omega}')d\omega' \tag{3.5}$$

Where the two reducing term, scattering and absorption, have been combined together in $\sigma_t = \sigma_a + \sigma_s$, called the *extinction coefficient*.

3.5.6 The diffusion approximation

The radiative transport equation 3.5 is a integro-differential equation with many degrees of freedom. As we stated in chapter 2, there are rendering techniques that numerically solve the equation in order to obtain a realistic result. However, analytical methods tend to use some approximations of the RTE, that hold well given specific conditions. The *diffusion approximation* is one of these approximations, and it is still widely used today since its introduction in the computer graphics community by IshimaruIshimaru [1997].

The assumption under the diffusion approximation is simple: given that in a physical medium there are a lot of scattering events, the beam of light quickly becomes isotropic. In fact, each one of the scattering events further blurs the light distribution, and as a result the distribution becomes more uniform as the number of scattering events increases. This has been proven to be a reasonable assumption even for highly anisotropic light sources (e.g. a focused laser beam) and phase functions.

When using the diffusion approximation, instead of using the extinction coefficient σ_t, we account for the contribution from the phase function by using the so-called *reduced extinction coefficient* σ'_t. It is defined as $\sigma'_t = \sigma_a + \sigma'_s$, with $\sigma'_s = \sigma_s(1-g)$. σ'_s Is called *reduced scattering coefficient*. The converse of the reduced scattering coefficient is called *mean free path* and represents the average distance that light travels in the medium before being absorbed or scattered.

The rationale behind this reduced coefficient is that a highly forward scattering material is virtually indistinguishable from a not-scattering material. So, for highly forward scattering materials ($g \approx 1$) the scattering coefficients reduces to zero. For highly backward scattering materials ($g \approx -1$), the scattering is accounted for twice as for an isotropic material (see table 3.2).

Coefficient	Backward Scattering ($g \approx -1$)	Isotropic ($g \approx 0$)	Forward Scattering ($g \approx 1$)
σ'_s	$2\sigma_s$	σ_s	0
σ'_t	$\sigma_a + 2\sigma_s$	$\sigma_a + \sigma_s$	σ_a

Table 3.2: Explicit scattering coefficients for different kinds of materials.

We leave to Ishimaru [1997] and Jensen et al. [2001] for the algebraic details of the calculation. Once we solve the diffusion equation, we obtain the following

formula for $\phi(\mathbf{x})$, the fluence of light in an infinite scattering medium.

$$\phi(\mathbf{x}) = \frac{\Phi}{4\pi D}\frac{e^{\sigma_{tr}r}}{r}$$

We recall that $\phi(\mathbf{x}) = \int_{4\pi} L(\mathbf{x}, \vec{\omega})d\vec{\omega}$. $r = \|\mathbf{x}\|$ is the distance from the point to the light source. The two coefficients D and σ_{tr} are called *diffusion coefficient* and *transmission coefficient* respectively. The two coefficients are defined as follows:

$$D = \frac{1}{3\sigma_t'}$$
$$\sigma_{tr} = \sqrt{3\sigma_a\sigma_t'} = \sqrt{\frac{\sigma_a}{D}}$$

This is the equation describe light propagation in an infinite medium, i.e. no surface interaction is considered. In order to derive an actual BSSRDF model from the diffusion approximation, *boundary conditions* must be considered. Jensen Jensen et al. [2001] derived an analytical model starting from this approximation of the RTE, while Frisvad Frisvad et al. [2013] uses a more complex approximation of the RTE. The two models are explained in the following sections.

3.5.7 Standard dipole model

The first model we describe is due to JensenJensen et al. [2001]. In their original paper, they used the diffusion approximation for light in an infinite medium described in the previous section. Starting from that, they derive an approximation that holds for light in a semi-infinite medium, i.e. light traveling in void hitting a planar slab of a translucent material.

As a boundary condition, we take the light coming *out* of the material. Light coming out of the material has a initial fluence ϕ_0. We assume then that the fluency decays linearly until a distance $z = 2AD$ from the surface, where it becomes zero. See Donner [2006] for the full derivation. D is the diffusion coefficient, while A is a corrective term that accounts for materials with mismatching

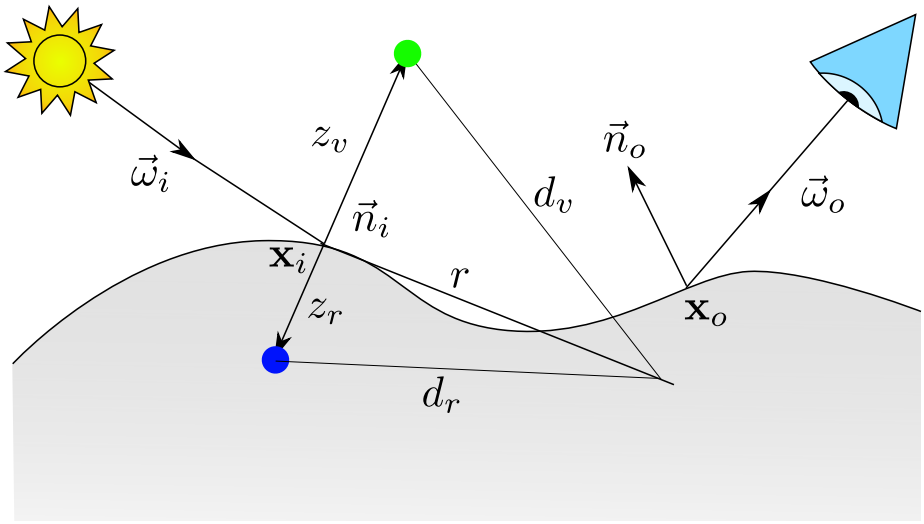

Figure 3.8: Setup for the standard dipole model.

indices of refraction:

$$\begin{aligned} A &= \frac{1 + F_{dr}}{1 - F_{dr}} \\ F_{dr} &= \int_{2\pi} R(\eta, \vec{n} \cdot \vec{\omega})(\vec{n} \cdot \vec{\omega}) d\vec{\omega} \end{aligned} \tag{3.6}$$

Where R is the Fresnel reflection term as defined in section 3.4.2, and $\eta = n_1/n_2$ is the ratio of the refraction indices. The Fresnel reflectance integral F_{dr} is usually approximated with an analytical expression:

$$F_{dr} = -\frac{1.440}{\eta^2} + \frac{0.710}{\eta} + 0.668 + 0.0036\eta$$

Given the boundary condition, we can then model the subsurface scattering in a point $\mathbf{x}_o$ with two small sources on the point, a configuration called a *dipole*. One source is placed beneath the surface, called the *real source*, while the other one is mirrored above the surface, called *virtual source*. The first source actually models the subsurface scattering effect, while the second one reduces the first in order to account for the boundary conditions and the extrapolation boundary. Refer to figure TODO for a visual detail on the setup.

The real source is placed one mean free path beneath the surface, at $z_r = 1/\sigma'_t$, while the virtual one is placed symmetrically according to the end of the boundary conditions, ad a distance $z_v = z_r + 4AD$. From z_r and z_v we can calculate the distances d_r and d_v from the entrance point $\mathbf{x}_i$. Given $r = \|\mathbf{x}_o - \mathbf{x}_i\|$, we obtain:

$$d_r = \sqrt{z_r^2 + r^2}$$
$$d_v = \sqrt{z_v^2 + r^2}$$

Given these constraints, we obtain an equation for the BSSRDF in a semi infinite medium:

$$S_d(\mathbf{x}_i, \vec{\omega}_i, \mathbf{x}_i, \vec{\omega}_o) = \frac{\alpha'}{4\pi^2}\left[\frac{z_r(1+\sigma_{tr}d_r)\ e^{-\sigma_{tr}d_r}}{d_r^3} + \frac{z_v(1+\sigma_{tr}d_v)\ e^{-\sigma_{tr}d_v}}{d_v^3}\right]$$

Where $\alpha' = \sigma'_s/\sigma'_t$ is called *reduced albedo*.

The model so far described was intended to model only the multiple scattering BSSRDF term, S_d. In order to obtain the full BSSRDF S, a single scattering term $S^{(1)}$ must be added. There are in literature many approaches ot model single scattering, that are too long to explain here. The final BSSRDF equation for the Jensen TODO model then becomes:

$$S(\mathbf{x}_i, \vec{\omega}_i, \mathbf{x}_o, \vec{\omega}_o) = S_d(\mathbf{x}_i, \vec{\omega}_i, \mathbf{x}_o, \vec{\omega}_o) + S^{(1)}(\mathbf{x}_i, \vec{\omega}_i, \mathbf{x}_o, \vec{\omega}_o)$$

Jensen et al. [2001] in their original paper describes and justify some corrections that need to be done to the model in order to make it work with generic surfaces, and on how to account for extensions like texture support. We will not describe these extensions here, remanding to the original paper for a description.

3.5.8 Directional dipole model

Various evolution to the standard dipole model have been proposed throughout the years. In this chapter, we will introduce the BSSRDF approximation called *directional dipole*, proposed by Frisvad et al. [2013]. In the standard

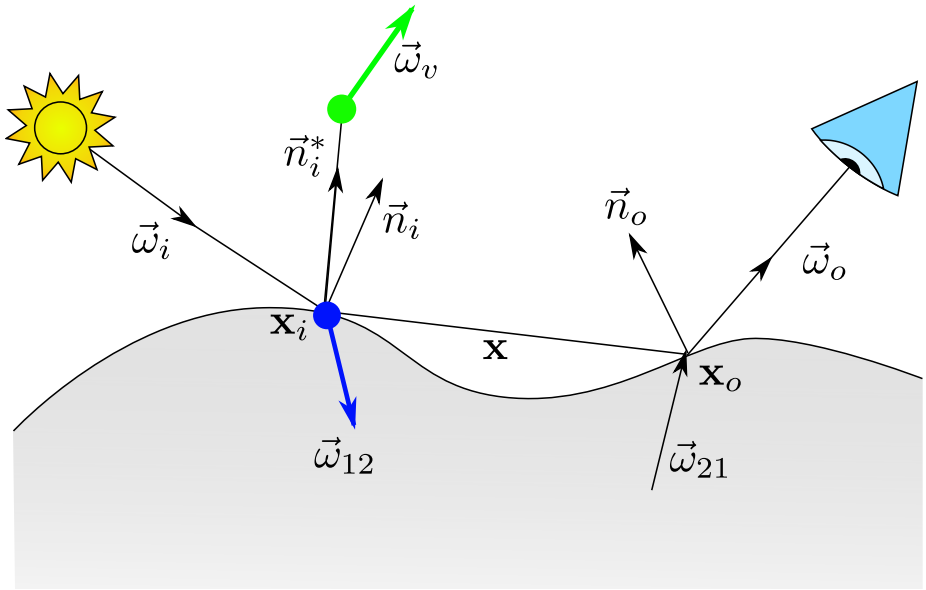

Figure 3.9: Setup for the directional dipole model.

dipole model, in fact, the diffusive part of the BSSRDF depends only on the distance between the point of incidence and the point of emergence, that is $S_d(\mathbf{x}_i, \vec{\omega}_i, \mathbf{x}_o, \vec{\omega}_o) = S_d(\|\mathbf{x}_o - \mathbf{x}_i\|)$.

The directional dipole model, based on the diffusion approximation, accounts for the direction of the incoming light in its calculations, in order to model the scattering effects more precisely. Moreover, the model, instead of splitting the BSSRDF in a multiple and single scattering term, splits the BSSRDF into a diffusive term S_d and a term $S_{\delta E}$, called *reduced intensity*, that can be computed using the delta-Eddington approximationJoseph et al. [1976]. The final BSSRDF thus becomes:

$$S(\mathbf{x}_i, \vec{\omega}_i, \mathbf{x}_o, \vec{\omega}_o) = T(\eta, \vec{\omega}_i)(S_d(\mathbf{x}_i, \vec{\omega}_i, \mathbf{x}_o) + S_{\delta E}(\mathbf{x}_i, \vec{\omega}_i, \mathbf{x}_o, \vec{\omega}_o))T(\eta, \vec{\omega}_o)$$

Where T are the Fresnel transmission coefficients for the incoming and outgoing directions. We note also that the diffusive part of the BSSRDF does not depend on the outgoing direction $\vec{\omega}_o$.

Diffusive BSSRDF

The diffusive part of the directional dipole model uses a first-order approximation of the RTE, that for a point light in an infinite medium gives the following fluence:

$$\phi(\mathbf{x}_o, \theta) = \frac{\Phi}{4\pi D} \frac{e^{\sigma_{tr} r}}{r} \left(1 + 3D \frac{1 + \sigma_{tr} r}{r} \cos\theta\right)$$

Where D and σ_{tr} are the two scattering coefficients defined beforehand, $r = \|\mathbf{x}_o\|$ and

$$\cos\theta = \frac{\mathbf{x} \cdot \vec{\omega}_{12}}{r}$$

Where $\vec{\omega}_{12}$ is the refracted vector as defined in 3.4.2. Comparing with equation TODO, we can see that we introduced a new term that depends on the angle between the refracted incoming light vector and the vector connecting incidence and emergence.

Using the diffusion approximation, we can first establish a relationship between the radiant exitance $M(\mathbf{x}_o)$ and the diffusive BSSRDF S'_d in an infinite medium:

$$\frac{dM(\mathbf{x}_o)}{d\Phi_i(\mathbf{x}, \vec{\omega}_i)} = T(\eta, \vec{\omega}_i) S'_d(\mathbf{x}_i, \vec{\omega}_i, \mathbf{x}_o)\ 4\pi C_\phi(1/\eta)$$

where $C_\phi(1/\eta)$ is related to the integral on the hemisphere of the fresnel coefficients. Using the definition of radiant exitance and inserting inside the classical iffusion approximation, we reach the diffusion formulation of the radiant exitance:

$$M(\mathbf{x}_o) = C_\phi(\eta)\phi(\mathbf{x}_o) + C_{\mathbf{E}}(\eta) D \vec{n}_o \cdot \nabla\phi(\mathbf{x}_o)$$

Again, $C_\phi(\eta)$ and $C_{\mathbf{E}}(\eta)$ are two terms that are related to the integration of the fresnel coefficients. Combining the three equations TODO, we reach the final

form for our diffusive BSSRDF in an infinite medium:

$$\begin{aligned} S'_d(\mathbf{x}, \vec{\omega}_{12}, r) &= \frac{1}{4C_\phi(1/\eta)} \frac{1}{4\pi^2} \frac{e^{-\sigma_{tr} r}}{r^3} \\ &\left[C_\phi(\eta) \left(\frac{r^2}{D} + 3(1+\sigma_{tr} r)\mathbf{x} \cdot \vec{\omega}_{12} \right) - \right. \\ &- C_{\mathbf{E}}(\eta) \Bigg(3D(1+\sigma_{tr} r)\, \vec{\omega}_{12} \cdot \vec{n}_o - \\ &\left. - \left((1+\sigma_{tr} r) + 3D \frac{3(1+\sigma_{tr} r) + (\sigma_{tr} r)^2}{r^2} \mathbf{x} \cdot \vec{\omega}_{12} \right) \mathbf{x} \cdot \vec{n}_o \Bigg) \right] \end{aligned} \tag{3.7}$$

Fresnel integrals

The two terms $C_\phi(\eta)$ and $C_{\mathbf{E}}(\eta)$ originally come from integrating the outgoing Fresnel transmittance over the whole outgoing hemisphere, weighted with a cosine term. The two functions are defined as follows:

$$\begin{aligned} C_\phi(\eta) &= \frac{1}{4\pi} \int_{2\pi} T(\eta, \vec{\omega})(\vec{n}_o \cdot \vec{\omega}) d\vec{\omega} \\ C_{\mathbf{E}}(\eta) &= \frac{3}{4\pi} \int_{2\pi} T(\eta, \vec{\omega})(\vec{n}_o \cdot \vec{\omega})^2 d\vec{\omega} \end{aligned} \tag{3.8}$$

These two integrals can be rearranged in order to express them in terms of reflectance instead of transmittance, recalling $R = 1 - T$.

$$\begin{aligned} C_\phi(\eta) &= \frac{1}{4\pi} \left(\pi - \int_{2\pi} R(\eta, \vec{\omega})(\vec{n}_o \cdot \vec{\omega}) d\vec{\omega} \right) = \frac{1}{4}(1 - 2C_1) \\ C_{\mathbf{E}}(\eta) &= \frac{3}{4\pi} \left(\frac{2\pi}{3} - \int_{2\pi} R(\eta, \vec{\omega})(\vec{n}_o \cdot \vec{\omega}) d\vec{\omega} \right) = \frac{1}{2}(1 - 3C_2) \end{aligned} \tag{3.9}$$

Even with this rearrangement the integral cannot be expressed in closed form. TODO and TODO use a convenient polynomial approximation for the two coeffiients C_1 and C_2, expressed as:

$$2C_1 \approx \begin{cases} +0.919317 - 3.4793\eta + 6.75335\eta^2 - 7.80989\eta^3 \\ \qquad +4.98554\eta^4 - 1.36881\eta^5 & \eta < 1 \\ -9.23372 + 22.2272\eta - 20.9292\eta^2 + 10.2291\eta^3 \\ \qquad -2.54396\eta^4 + 0.254913\eta^5 & \eta \geq 1 \end{cases}$$

$$3C_2 \approx \begin{cases} 0.828421 - 2.62051\eta + 3.36231\eta^2 - 1.95284\eta^3 \\ \qquad +0.236494\eta^4 + 0.145787\eta^5 & \eta < 1 \\ -1641.1 + \frac{135.926}{\eta^3} - \frac{656.175}{\eta^2} + \frac{1376.53}{\eta} + 1213.67\eta \\ \qquad -568.556\eta^2 + 164.798\eta^3 \\ \qquad -27.0181\eta^4 + 1.91826\eta^5 & \eta \geq 1. \end{cases}$$

Boundary conditions

As the name implies, also for the directional dipole we model the boundary conditions on the material interface using a dipole. In this case, however, instead of using two point light sources, we use two ray sources, a real and a virtual one. As in the standard dipole, the source is displaced towards the normal of a distance d_e. In the case of the standard dipole, we use $2D$, that becomes $2AD$ in the case of mismatching indices of refraction on the interface. In the case of the directional dipole, we use

$$d_e = \frac{2.131D}{\sqrt{\alpha'}}$$

Where we recall $\alpha' = \sigma'_s/\sigma'_t$ as the reduced albedo. This result have been proven TODO to be consistent with numerical simulations of the RTE. In addition, the A term is modified using the hemispheric Fresnel integrals:

$$A(\eta) = \frac{1 - C_{\mathbf{E}}(\eta)}{2C_\phi(\eta)}$$

As the standard dipole, the directional dipole assumes a semi-infinite medium given the previous boundary conditions. In order to relax this assumptions, we need to further extend the model in order to reduce undesired effects. One first modification proposed by TODO is to use a modified tangent plane defined by the normal $\vec{n}_i^*$ to mirror the real source towards the mirror light source, instead of the obvious one defined by $\vec{n}_i$. We define the modified normal as follows:

$$\vec{n}_i^* = \begin{cases} \vec{n}_i & \text{for} \mathbf{x}_o = \mathbf{x}_i \\ \dfrac{\mathbf{x}_o - \mathbf{x}_i}{\|\mathbf{x}_o - \mathbf{x}_i\|} \times \dfrac{\vec{n}_i \times (\mathbf{x}_o - \mathbf{x}_i)}{\|\vec{n}_i \times (\mathbf{x}_o - \mathbf{x}_i)\|} & \text{otherwise} \end{cases}$$

Another important modification is the distance to the real source. In the standard dipole, we used $d_r = \sqrt{z_r^2 + r^2}$, with $z_r = 1/\sigma_t'$, which is the average distance a photon travels within the material before being absorbed or scattered. The problem of this definition is that it introduces a singularity in $r = 0$. Moreover, the standard dipole becomes fairly imprecise when r is small, overestimating the overall effect. In order to avoid these problems, Frisvad et al. [2013] proposed a more complicated definition of d_r that matches simulation of transport theory more closely. For the details, see Appendix B in the original paper. d_r is defined as follows, recalling $\sigma_t = \sigma_s + \sigma_a$:

$$d_r^2 = \begin{cases} r^2 + D\mu_0(D\mu_0 - 2d_e \cos\beta) & \mu_0 \geq 0 \text{ (frontlit)} \\ r^2 + \dfrac{1}{(3\sigma_t)^2} & \mu_0 < 0 \text{ (backlit)} \end{cases}$$

Where $\mu_0 = -\vec{\omega}_{12} \cdot \vec{n}_o$ is an indicator if the point $\mathbf{x}_o$ is frontlit or backlit. β is a geometry term that is evaluated as:

$$\cos\beta = -\sqrt{\frac{r^2 - (\mathbf{x} \cdot \vec{\omega}_{12})^2}{r^2 + d_e^2}}$$

Combining all the corrections seen so far, we can write the final form of our BSSRDF model, that is a combination of the real source term minus the virtual source term:

$$S_d(\mathbf{x}_i, \vec{\omega}_i, \mathbf{x}_o) = S_d'(\mathbf{x}_o - \mathbf{x}_i, \vec{\omega}_{12}, d_r) - S_d'(\mathbf{x}_o - \mathbf{x}_v, \vec{\omega}_v, d_v)$$

Where the extra coefficients are defined as follows:

$$\begin{aligned} x_v &= x_i + 2Ad_e\vec{n}_i^* \\ \vec{\omega}_v &= \vec{\omega}_{12} - 2(\vec{\omega}_{12} \cdot \vec{n}_i^*)\vec{n}_i^* \\ d_v &= \|x_o - x_v\| \end{aligned}$$

The directional dipole model described in this chapter, gives a better result that the standard dipole, at the extra price of add calculations. In particular, the model improves the previous ones for highly forward scattering materials, where it is sensibly close to the path traced result. The goals of this thesis is to provide a real-time implementation of it. Given this theoretical introduction, in the next section we will describe our contribution in order to breakdown the problems and the issues of a real-time implementation.

Chapter 4

Method

In this chapter, the goal is to solve the problem that we have presented, i.e. rendering translucent materials efficiently using the directional dipole. First of all, we will start this chapter with a list of constraints and assumptions that we will use to devise our method. Secondly, we will give a theoretical justification of our method, deriving a discretization of the rendering equation that can be actually implemented in a GPU environment. Then, we will discuss some possible sampling patterns and how they could possibly improve the results of the final rendering. Then, we will introduce how the actual scattering parameters are acquired in an experimental environment, in order to obtain a plausible result.

4.1 Constraints and assumptions

Quality constraints

1. Close as much as possible to a path traced solution.
2. work with the less amount as possible of provided data, i.e. only the position data and eventually the normals should be provided in order for the method to run. In particular, no uv mapping should be necessary for the method to run.

3. If the quality is not reachable within one frame, converge towards a result in a reasonable amount of time. Techniuqes should be used to fake the required quality in order to approximate the itnermediate result.
4. flexibility: integrable in a engine-ready environment, or adaptable to different shading techniques (forward and deferred rendering)
5. tweakable: the quality / performance tradeoff should be set by a potential artist, and with the fewest number of parameters as possible.

Performance assumptions

1. Maintain a reasonable performance under changing light conditions, deformations and change of parameters, with little or none performance parameters
2. As less as dependent as possible from the geometrical complexity of the model.
3. As less as dependent from the screen resolution.
4. Being real-time, i.e. one frame should take less that 100 ms (10 FPS) to render. The ideal result would be to reach a rendering time of less than 16ms
5. Employ the advantages of the directional dipole model to improve performance.
6. Support a certain number of directional and point lights (up to 3 to 5 pixel lights, as in commercial enginesUnity [2012])

4.2 Method overview

TODO overview

Going into the mathematical details the idea is to take the integral form of the rendering equation (equation 3.3):

$$L_o(\mathbf{x}_o, \vec{\omega}_o) = L_e(\mathbf{x}_i, \vec{\omega}_i) + \int_A \int_{2\pi} S(\mathbf{x}_i, \vec{\omega}_i, \mathbf{x}_o, \vec{\omega}_o) L_i(\mathbf{x}_i, \vec{\omega}_i) V(\mathbf{x}_i)(\vec{n}_i \cdot \vec{\omega}_i) d\vec{\omega}_i dA_i$$

First of all, we make the assumption of a body that is not emitting light: all the radiance from the body comes from an external source. This assumption can be trivially relaxed and implemented, but to simplify the equation in this chapter we will exclude it from the calculations. Secondly, we limit ourselves to the case of one directional light, treating the case of a point light later as an extension. The directional light direction $\vec{\omega}_l$ and radiance $L_d\ \delta(\vec{\omega}_d)$.

Under the first assumption, equation 3.3 becomes:

$$L_o^D(\mathbf{x}_o, \vec{\omega}_o) = \int_A \int_{2\pi} S(\mathbf{x}_i, \vec{\omega}_i, \mathbf{x}_o, \vec{\omega}_o) L_d\ \delta(\vec{\omega}_l)\ V(\mathbf{x}_i)(\vec{n}_i \cdot \vec{\omega}_i) d\vec{\omega}_i dA_i$$
$$L_o^D(\mathbf{x}_o, \vec{\omega}_o) = \int_A S(\mathbf{x}_i, \vec{\omega}_l, \mathbf{x}_o, \vec{\omega}_o) L_d V(\mathbf{x}_i)(\vec{n}_i \cdot \vec{\omega}_l) dA_i$$

In this way, we remove the internal integral. Then, in order to make a feasible calculation, we need to discretize the other integral as well. We imagine to have a set of N points on the surface. We assume that each one of these points is visible from the light source (so we can get rid of the $V(\mathbf{x}_i)$ term). We will discuss in the implementation section how to make sure that all these points are visible. Each one of these points has an associated area A_i, so that we can write:

$$L_o^D(\mathbf{x}_o, \vec{\omega}_o) = L_d \sum_{i=1}^{N} S(\mathbf{x}_i, \vec{\omega}_l, \mathbf{x}_o, \vec{\omega}_o)(\vec{n}_i \cdot \vec{\omega}_l) A_i \tag{4.1}$$

Now, instead of using all the points on the surface, we consider only the points within a certain radius r^* from the point $\mathbf{x}_o$. This is reasonable because because the dominating term in the directional dipole is $e^{-\sigma_{tr} r}$, so after a certain critical radius the contribution from the other points becomes negligible. Assuming the points are distributed uniformly on the circle, we obtain the following area for a point:

$$A_i = \frac{A_c}{N\ (\vec{n}_i \cdot \vec{\omega}_l)}$$

Where $A_c = \pi(r^*)^2$ is the area of the circle. And, by inserting into equation

4.1, we obtain:

$$L_o^D(\mathbf{x}_o, \vec{\omega}_o) = L_d \frac{A_c}{N} \sum_{i=1}^{N} S(\mathbf{x}_i, \vec{\omega}_l, \mathbf{x}_o, \vec{\omega}_o) \tag{4.2}$$

That is our final approximation for a directional light. For a point light, following the exact same steps, we reach a similar solution. We recall that a point light is defined by an intensity I_p and a source point $\mathbf{x}_p$:

$$L_o^P(\mathbf{x}_o, \vec{\omega}_o) = I_p \frac{A_c}{N} \sum_{i=1}^{N} \frac{S(\mathbf{x}_i, \frac{\mathbf{x}_p - \mathbf{x}_i}{\|\mathbf{x}_p - \mathbf{x}_i\|}, \mathbf{x}_o, \vec{\omega}_o)}{\|\mathbf{x}_p - \mathbf{x}_i\|^2} \tag{4.3}$$

And, since the radiance is linearly summable, we can combine the contribution from an arbitrary number of $P_1, P_2 ... P_p$ point sources and $D_1, D_2 ... D_d$ directional sources:

$$\begin{aligned} & L_o(\mathbf{x}_o, \vec{\omega}_o) = \\ & = \sum_{k=1}^{p} L_o^{P_k}(\mathbf{x}_o, \vec{\omega}_o) + \sum_{k=1}^{d} L_o^{D_k}(\mathbf{x}_o, \vec{\omega}_o) \\ & = \frac{A_c}{N} \left[\sum_{k=1}^{p} I_p^k \sum_{i=1}^{N} \frac{S(\mathbf{x}_i, \frac{\mathbf{x}_p^k - \mathbf{x}_i}{\|\mathbf{x}_p^k - \mathbf{x}_i\|}, \mathbf{x}_o, \vec{\omega}_o)}{\|\mathbf{x}_p^k - \mathbf{x}_i\|^2} + \sum_{k=1}^{d} L_d^k \sum_{i=1}^{N} S(\mathbf{x}_i, \vec{\omega}_l^k, \mathbf{x}_o, \vec{\omega}_o) \right] \end{aligned} \tag{4.4}$$

4.3 Sampling patterns

As we discussed in the previous section, the BSSRDF function for the directional dipole is dominated by an exponential decay. So, it is more probable to find points that contribute more to the BSSRDF if we take points closer to the evaluation point $\mathbf{x}_o$. However, our assumption of uniform areas does not hold anymore, so we need to modify the previous equations in order to account for the non-linear sampling.

Assuming to have number generator that can generate numbers on a disc, we can create an exponentially distributed disc by rejection sampling. The probability distribution is:

$$pdf(x) = \sigma_{tr} e^{-\sigma_{tr} x}$$

We will give more detail on the process later. The radius of the point $\mathbf{x}_i$ is

$$r_i = \|\mathbf{x}_o^{proj} - \mathbf{x}_i^{proj}\|$$

Where the two points have been projected on the circle. See figure X for more details. So now we have a new normalization term to include in order to scale back the result. So, we need now to divide by $exp(-\sigma_{tr} r_i)$ each sample. The new equation for a directional light then becomes:

$$\hat{L}_o^D(\mathbf{x}_o, \vec{\omega}_o) = L_d \frac{A_c}{N} \sum_{i=1}^{N} S(\mathbf{x}_i, \vec{\omega}_l, \mathbf{x}_o, \vec{\omega}_o) e^{-\sigma_{tr} r_i}$$

The other two equations TODO and TODO change accordingly:

$$\hat{L}_o^P(\mathbf{x}_o, \vec{\omega}_o) = I_p \frac{A_c}{N} \sum_{i=1}^{N} \frac{S(\mathbf{x}_i, \frac{\mathbf{x}_p - \mathbf{x}_i}{\|\mathbf{x}_p - \mathbf{x}_i\|}, \mathbf{x}_o, \vec{\omega}_o)}{\|\mathbf{x}_p - \mathbf{x}_i\|^2} e^{-\sigma_{tr} r_i}$$

$$\begin{aligned}
&\hat{L}_o(\mathbf{x}_o, \vec{\omega}_o) = \\
&= \sum_{k=1}^{p} L_o^{P_k}(\mathbf{x}_o, \vec{\omega}_o) + \sum_{k=1}^{d} L_o^{D_k}(\mathbf{x}_o, \vec{\omega}_o) \\
&= \frac{A_c}{N} \left[\sum_{k=1}^{p} I_p^k \sum_{i=1}^{N} \frac{S(\mathbf{x}_i, \frac{\mathbf{x}_p^k - \mathbf{x}_i}{\|\mathbf{x}_p^k - \mathbf{x}_i\|}, \mathbf{x}_o, \vec{\omega}_o)}{\|\mathbf{x}_p^k - \mathbf{x}_i\|^2} e^{-\sigma_{tr} r_i} + \sum_{k=1}^{d} L_d^k \sum_{i=1}^{N} S(\mathbf{x}_i, \vec{\omega}_l^k, \mathbf{x}_o, \vec{\omega}_o) e^{-\sigma_{tr} r_i} \right]
\end{aligned} \tag{4.5}$$

4.4 Parameter acquisition

When rendering translucent materials, it is important that we have the right scattering properties, in order to match the appearance of real world objects. The scattering parameters may be tweaked by the artist and set up manually,

but this is a long process since the the scattering properties are not directly related to material appearance. In order to avoid this problems, the scattering parameters are measured from samples taken from real world objects. In this section, we will give an overview of two methods used to estimate the scattering parameters.

The first method was presented alongside the standard dipole model by Jensen et al. [2001]. The measurement apparatus consists of a series of lenses that focus the light on the sample. The light power Φ is measured by calibrating the sensor with a spectralon sample. A picture of the sample is then acquired at different exposure, in order to build an high dynamic range image. This is necessary since the scattering decays exponentially, so a high range is needed to have meaningful measurements. The measured data are then fitted to diffusion theory in order to obtain the scattering coefficients. Due to the nature of the measurement, it is not possible to measure the mean cosine g of the material, but only the reduced scattering coefficient $\sigma'_s = \sigma_s(1-g)$ and the absorption coefficient σ_a. This measurement model uses the diffusion approximation to work, so it shares the same limitations: it is valid only for materials where $\sigma_a \ll \sigma_s$.

The second method, proposed by Narasimhan et al. [2006] proposes a method to measure the scattering coefficient by dilution. The assumption is that water does not interfere with the scattering properties of the materials dissolved within it for small distances (less than 50 cm). Naturally, the material needs then to be already in a liquid form, or to be a powder that can be easily dissolved in water. The setup of the experiment is a box full of water with a camera and an area light. High dynamic range picture of the material dissolved in water are then taken, and the scattering coefficients can be measured with a low error. Various measurements at different concentrations are needed in order to get an effective measurement of the coefficients, but then the coefficients can be extrapolated for any concentration.

Some of the scattering properties measured thanks to this method are reported in table 4.1. This coefficients will be used throughout the report when referencing to a specific material.

Material	Absorption, σ_a			Scattering, σ_s			Mean cosine, g			η	Source
	R	G	B	R	G	B	R	G	B		
Apple	0.0030	0.0034	0.0046	2.29	2.39	1.97	-	-	-	1.3	J
Ketchup	0.061	0.97	1.45	0.18	0.07	0.03	-	-	-	1.3	J
Marble	0.0021	0.0041	0.0071	2.19	2.62	3.00	-	-	-	1.5	J
Potato	0.0024	0.0090	0.12	0.68	0.70	0.55	-	-	-	1.3	J
Whole milk	0.0011	0.0024	0.014	2.55	3.21	3.77	-	-	-	1.3	J
Coffee	0.1669	0.2287	0.3078	0.2707	0.2828	0.297	0.907	0.896	0.88	1.3	N
Soy milk	0.0001	0.0005	0.0034	0.2433	0.2714	0.4563	0.873	0.858	0.832	1.3	N
Wine (merlot)	0.7586	1.6429	1.9196	0.0053	0	0	0.974	0	0	1.3	N
Beer (Budweiser)	0.1449	0.3141	0.7286	0.0037	0.0069	0.0074	0.917	0.956	0.982	1.3	N
White grapefruit juice	0.0096	0.0131	0.0395	0.3513	0.3669	0.5237	0.548	0.545	0.565	1.3	N

Table 4.1: Scattering material parameters estimated using different methods. For the source field, `J` materials come from Jensen et al. [2001], while `N` materials come from Narasimhan et al. [2006]. Note that the materials measured with the technique proposed in Jensen et al. [2001] are without the g coefficient.

Chapter 5

Results

Bibliography

Michael Ashikmin, Simon Premože, and Peter Shirley. A microfacet-based brdf generator. In *Proceedings of the 27th Annual Conference on Computer Graphics and Interactive Techniques*, SIGGRAPH '00, pages 65–74, New York, NY, USA, 2000. ACM Press/Addison-Wesley Publishing Co. URL `http://dx.doi.org/10.1145/344779.344814`.

Jesper Børlum, Brian Bunch Christensen, Thomas Kim Kjeldsen, Peter Trier Mikkelsen, Karsten Østergaard Noe, Jens Rimestad, and Jesper Mosegaard. Sslpv: Subsurface light propagation volumes. In *Proceedings of the ACM SIGGRAPH Symposium on High Performance Graphics*, HPG '11, pages 7–14, New York, NY, USA, 2011. ACM. URL `http://doi.acm.org/10.1145/2018323.2018325`.

Michael F. Cohen, John Wallace, and Pat Hanrahan. *Radiosity and Realistic Image Synthesis*. Academic Press Professional, Inc., San Diego, CA, USA, 1993.

Carsten Dachsbacher and Marc Stamminger. Translucent shadow maps. In *Proceedings of the 14th Eurographics Workshop on Rendering*, EGRW '03, pages 197–201, Aire-la-Ville, Switzerland, Switzerland, 2003. Eurographics Association. URL `http://dl.acm.org/citation.cfm?id=882404.882433`.

Eugene D'Eon. A better dipole (a publicly available manuscript). Technical report, -, 2012. URL `.http://www.eugenedeon.com/papers/betterdipole.pdf.`

Eugene D'Eon and Geoffrey Irving. A quantized-diffusion model for rendering translucent materials. In *ACM SIGGRAPH 2011 Papers*, SIGGRAPH '11, pages 56:1–56:14, New York, NY, USA, 2011. ACM. URL `http://doi.acm.org/10.1145/1964921.1964951`.

Eugene d'Eon, David Luebke, and Eric Enderton. Efficient rendering of human skin. In *Proceedings of the 18th Eurographics Conference on Rendering Techniques*, EGSR'07, pages 147–157, Aire-la-Ville, Switzerland, Switzerland, 2007. Eurographics Association. URL http://dx.doi.org/10.2312/EGWR/EGSR07/147-157.

Agns Desolneux, Lionel Moisan, and Jean-Michel Morel. *From Gestalt Theory to Image Analysis: A Probabilistic Approach.* Springer Publishing Company, Incorporated, 1st edition, 2007.

Craig Donner and Henrik Wann Jensen. Light diffusion in multi-layered translucent materials. In *ACM SIGGRAPH 2005 Papers*, SIGGRAPH '05, pages 1032–1039, New York, NY, USA, 2005. ACM. URL http://doi.acm.org/10.1145/1186822.1073308.

Craig Donner, Jason Lawrence, Ravi Ramamoorthi, Toshiya Hachisuka, Henrik Wann Jensen, and Shree Nayar. An empirical bssrdf model. *ACM Trans. Graph.*, 28(3):30:1–30:10, July 2009. URL http://doi.acm.org/10.1145/1531326.1531336.

Craig Steven Donner. *Towards Realistic Image Synthesis of Scattering Materials.* PhD thesis, University of California, San Diego, La Jolla, CA, USA, 2006. AAI3226771.

Julie Dorsey, Alan Edelman, Henrik Wann Jensen, Justin Legakis, and Hans Køhling Pedersen. Modeling and rendering of weathered stone. In *Proceedings of the 26th Annual Conference on Computer Graphics and Interactive Techniques*, SIGGRAPH '99, pages 225–234, New York, NY, USA, 1999. ACM Press/Addison-Wesley Publishing Co. URL http://dx.doi.org/10.1145/311535.311560.

Raanan Fattal. Participating media illumination using light propagation maps. *ACM Trans. Graph.*, 28(1):7:1–7:11, February 2009. URL http://doi.acm.org/10.1145/1477926.1477933.

J. R. Frisvad, T. Hachisuka, and T. K. Kjeldsen. Directional dipole for subsurface scattering in translucent materials. Technical report, DTU Compute, 2013. URL http://www2.imm.dtu.dk/pubdb/p.php?6646. Unpublished manuscript.

Akira Ishimaru. *Wave propagation and scattering in random media.* IEEE, 1997.

Henrik Wann Jensen and Juan Buhler. A rapid hierarchical rendering technique for translucent materials. *ACM Trans. Graph.*, 21(3):576–581, July 2002. URL http://doi.acm.org/10.1145/566654.566619.

Henrik Wann Jensen and Per H. Christensen. Efficient simulation of light transport in scenes with participating media using photon maps. In *Proceedings of the 25th Annual Conference on Computer Graphics and Interactive Techniques*, SIGGRAPH '98, pages 311–320, New York, NY, USA, 1998. ACM. URL `http://doi.acm.org/10.1145/280814.280925`.

Henrik Wann Jensen, Stephen R. Marschner, Marc Levoy, and Pat Hanrahan. A practical model for subsurface light transport. In *Proceedings of the 28th Annual Conference on Computer Graphics and Interactive Techniques*, SIGGRAPH '01, pages 511–518, New York, NY, USA, 2001. ACM. URL `http://doi.acm.org/10.1145/383259.383319`.

Jorge Jimenez, Veronica Sundstedt, and Diego Gutierrez. Screen-space perceptual rendering of human skin. *ACM Trans. Appl. Percept.*, 6(4):23:1–23:15, October 2009. URL `http://doi.acm.org/10.1145/1609967.1609970`.

J. H. Joseph, W. J. Wiscombe, and J. A. Weinman. The delta-Eddington approximation for radiative flux transfer. *Journal of Atmospheric Sciences*, 33:2452–2459, December 1976.

Anton Kaplanyan and Carsten Dachsbacher. Cascaded light propagation volumes for real-time indirect illumination. In *Proceedings of the 2010 ACM SIGGRAPH Symposium on Interactive 3D Graphics and Games*, I3D '10, pages 99–107, New York, NY, USA, 2010. ACM. URL `http://doi.acm.org/10.1145/1730804.1730821`.

Hendrik P. A. Lensch, Michael Goesele, Philippe Bekaert, Jan Kautz, Marcus A. Magnor, Jochen Lang, and Hans-Peter Seidel. Interactive rendering of translucent objects. In *Proceedings of the 10th Pacific Conference on Computer Graphics and Applications*, PG '02, pages 214–, Washington, DC, USA, 2002. IEEE Computer Society. URL `http://dl.acm.org/citation.cfm?id=826030.826632`.

Tom Mertens, J. Kautz, P. Bekaert, F. Van Reeth, and H.-P. Seidel. Efficient rendering of local subsurface scattering. In *Computer Graphics and Applications, 2003. Proceedings. 11th Pacific Conference on*, pages 51–58, Oct 2003a.

Tom Mertens, Jan Kautz, Philippe Bekaert, Hans-Peter Seidelz, and Frank Van Reeth. Interactive rendering of translucent deformable objects. In *Proceedings of the 14th Eurographics Workshop on Rendering*, EGRW '03, pages 130–140, Aire-la-Ville, Switzerland, Switzerland, 2003b. Eurographics Association. URL `http://dl.acm.org/citation.cfm?id=882404.882423`.

Rosana Montes Soldado and Carlos Ureña Almagro. An overview of brdf models. -, -:–, 2012.

Srinivasa G. Narasimhan, Mohit Gupta, Craig Donner, Ravi Ramamoorthi, Shree K. Nayar, and Henrik Wann Jensen. Acquiring scattering properties of participating media by dilution. *ACM Trans. Graph.*, 25(3):1003–1012, July 2006. URL http://doi.acm.org/10.1145/1141911.1141986.

Matt Pharr and Pat Hanrahan. Monte carlo evaluation of non-linear scattering equations for subsurface reflection. In *Proceedings of the 27th Annual Conference on Computer Graphics and Interactive Techniques*, SIGGRAPH '00, pages 75–84, New York, NY, USA, 2000. ACM Press/Addison-Wesley Publishing Co. URL http://dx.doi.org/10.1145/344779.344824.

M.A. Shah, J. Konttinen, and S. Pattanaik. Image-space subsurface scattering for interactive rendering of deformable translucent objects. *Computer Graphics and Applications, IEEE*, 29(1):66–78, Jan 2009.

Jos Stam. Multiple scattering as a diffusion process. In PatrickM. Hanrahan and Werner Purgathofer, editors, *Rendering Techniques 1995*, Eurographics, pages 41–50. Springer Vienna, 1995. URL http://dx.doi.org/10.1007/978-3-7091-9430-0_5.

Anna Tomaszewska and Krzysztof Stefanowski. Real-time spherical harmonics based subsurface scattering. In Aurélio Campilho and Mohamed Kamel, editors, *Image Analysis and Recognition*, volume 7324 of *Lecture Notes in Computer Science*, pages 402–409. Springer Berlin Heidelberg, 2012. URL http://dx.doi.org/10.1007/978-3-642-31295-3_47.

Unity. *Unity Manual: Forward Rendering Path Details*, 2012. URL http://docs.unity3d.com/Manual/RenderTech-ForwardRendering.html.

Yajun Wang, Jiaping Wang, Nicolas Holzschuch, Kartic Subr, Jun-Hai Yong, and Baining Guo. Real-time rendering of heterogeneous translucent objects with arbitrary shapes. *Comput. Graph. Forum*, 29(2):497–506, 2010. URL http://dblp.uni-trier.de/db/journals/cgf/cgf29.html#WangWHSYG10.